Romero-Mangado, Jaione; Nordlund, Dennis; Soberon, Felipe; Deane, Graham; Maughan, Kevin; Sainio, Sami; Singh, Gurusharan; Daniels, Stephen; Saunders, Ian T.; Loftus, David; Meyyappan, M.; Koehne, Jessica; Gandhiraman, Ram P.

Morphological and chemical changes of aerosolized E. coli treated with a dielectric barrier discharge

Published in:
Biointerphases

DOI:
10.1116/1.4941367

Published: 01/03/2016

Document Version
Publisher's PDF, also known as Version of record

Please cite the original version:
Romero-Mangado, J., Nordlund, D., Soberon, F., Deane, G., Maughan, K., Sainio, S., Singh, G., Daniels, S., Saunders, I. T., Loftus, D., Meyyappan, M., Koehne, J., & Gandhiraman, R. P. (2016). Morphological and chemical changes of aerosolized E. coli treated with a dielectric barrier discharge. *Biointerphases*, *11*(1), Article 011009. https://doi.org/10.1116/1.4941367

Morphological and chemical changes of aerosolized E. coli treated with a dielectric barrier discharge

Jaione Romero-Mangado, Dennis Nordlund, Felipe Soberon, Graham Deane, Kevin Maughan, Sami Sainio, Gurusharan Singh, Stephen Daniels, Ian T. Saunders, David Loftus, M. Meyyappan, Jessica Koehne, and Ram P. Gandhiraman

Citation: Biointerphases **11**, 011009 (2016); doi: 10.1116/1.4941367

View online: https://doi.org/10.1116/1.4941367

View Table of Contents: http://avs.scitation.org/toc/bip/11/1

Published by the American Vacuum Society

Morphological and chemical changes of aerosolized *E. coli* treated with a dielectric barrier discharge

Jaione Romero-Mangado
NASA Ames Research Center, Moffett Field, California 94035

Dennis Nordlund
Stanford Synchrotron Radiation Lightsource, SLAC National Accelerator Laboratory, Menlo Park, California 94025

Felipe Soberon, Graham Deane, and Kevin Maughan
Novaerus, Inc., 111 N. Canal St. Suite 165, Chicago, Illinois 60606

Sami Sainio
Department of Electrical Engineering and Automation, School of Electrical Engineering, Aalto University, Espoo 02150, Finland

Gurusharan Singh and Stephen Daniels
National Center for Plasma Science and Technology, Dublin City University, Dublin 9, Ireland

Ian T. Saunders, David Loftus, M. Meyyappan, and Jessica Koehne
NASA Ames Research Center, Moffett Field, California 94035

Ram P. Gandhiraman[a)]
NASA Ames Research Center, Moffett Field, California 94035 and Universities Space Research Association, Mountain View, California 94043

(Received 26 October 2015; accepted 22 January 2016; published 12 February 2016)

This study presents the morphological and chemical modification of the cell structure of aerosolized *Escherichia coli* treated with a dielectric barrier discharge (DBD). Exposure to DBD results in severe oxidation of the bacteria, leading to the formation of hydroxyl groups and carbonyl groups and a significant reduction in amine functionalities and phosphate groups. Near edge x-ray absorption fine structure (NEXAFS) measurements confirm the presence of additional oxide bonds upon DBD treatment, suggesting oxidation of the outer layer of the cell wall. Electron microscopy images show that the bacteria undergo physical distortion to varying degrees, resulting in deformation of the bacterial structure. The electromagnetic field around the DBD coil causes severe damage to the cell structure, possibly resulting in leakage of vital cellular materials. The oxidation and chemical modification of the bacterial components are evident from the Fourier transform infrared spectroscopy and NEXAFS results. The bacterial reculture experiments confirm inactivation of airborne *E.* coli upon treating with DBD. [http://dx.doi.org/10.1116/1.4941367]

I. INTRODUCTION

Cold atmospheric pressure plasmas have gained significant recognition in recent years in the field of healthcare, for example, in the treatment of living cells, sterilization of medical devices, wound healing, and blood coagulation.[1–3] The plasmas are nontoxic, provide rapid and continuous antibacterial treatment, leave no residues to clean up, and are easy to scale up, compared to other approaches. They present an advance over radio frequency high vacuum plasmas used in the above applications by eliminating the need for high vacuum pumps and power systems. While the effects of atmospheric pressure plasma on surface bound bacteria have been well studied, their use for treating airborne microorganisms has received much less attention[4–7] and this is the subject of the present study.

The most commonly used technologies for air cleaning include high efficiency particulate air filters, UV irradiation, chemicals (spray, gel), and gas spray (ozone, hydrogen peroxide).[8–13] These methods, while popular, often provide suboptimal outcomes such as creating bacterial resistance, developing mutagenic outcomes if bacteria are underexposed, and are responsible for numerous health hazards when operated incorrectly (for example, radiation exposure in the case of UV). Prolonged exposure to radiation could cause skin irritation.[14,15] UV irradiation for air disinfection comes in several forms, including full intensity irradiation of a room with no occupants and shielded UV irradiation done with no restrictions on human occupation.[16] One of the biggest drawbacks of UV irradiation is that it requires direct "line of sight" exposure to be effective; "shadowing" may occur when used to treat airborne bacteria, a process whereby the exposed upper layers of a bacterial cluster are deactivated while providing a protective shield for the

[a)]Electronic mail: ramprasad.gandhiraman@nasa.gov

bacteria below them, particularly those that form biofilms.[17] While the above technologies are often used on their own, they may be combined; for example, a combination of high efficiency particulate air filters with UV irradiation was shown to be effective in reducing 60% of the bioaerosols in a contaminated room.[18] Pal *et al.* reported titanium dioxide nanoparticle mediated photocatalytic inactivation of airborne *Escherichia coli* in a continuous flow reactor[19,20] and fluorescent light inactivation of Gram negative and Gram positive bacteria.[21] Kowalski *et al.* reported killing *E. coli* in 10–480 s using high concentrations of ozone (300–631 ppm).[22]

Dielectric barrier discharge (DBD) is a popular approach to produce cold plasmas at atmospheric pressure used in air treatment.[4–7] In this work, we have probed the effect of DBD on the surface chemical and topographical changes of the bacteria. Though the individual microorganisms will have different chemical composition and cell structure, we have taken a simple Gram negative model bacteria *E. coli* for this study. Here, we present a DBD based technology using a novel electrode for generating the discharge for possible air hygiene applications. *E. coli* was chosen as a model organism for this study because of its prevalence in many human occupied spaces, and its rod-like structure makes it easier to see morphological surface changes. Fourier transform infrared spectroscopy (FTIR) and x ray absorption spectroscopy (XAS) [near edge x ray absorptions fine structure (NEXAFS)] were used for the detailed analysis of the chemical composition changes upon DBD exposure.

II. EXPERIMENT

A. Materials

E. coli (Migula) Castellani and Chalmers (ATCC 25922) was rehydrated in 1 ml of tryptic soy broth (BD 211825). The aliquot was aseptically transferred into a tube containing 5 ml of tryptic soy broth and incubated overnight with shaking at 37 °C. The bacterial suspension was then centrifuged at 1000 rpm for 10 min, the supernatant was discarded, and the cells were washed down four times with distilled water. The cell culture was transferred to a tube and vortexed to resuspend the bacterial cell pellet in distilled water.

B. Experimental setup

The DBD system (NV200, Novaerus, Inc.) electrode consists of two coaxial cylindrical mesh coils (304 stainless steel, 0.2 mm diameter wire) separated by a dielectric, borosilicate glass tube (Fig. 1). The glass tube has the following dimensions: 80 mm length, 22.5 mm internal diameter, and 28 mm outer diameter. A high alternating voltage, 4 kV, is applied to the coils via a step-up transformer. A fan inside the NV200 unit is used to draw the air containing bioaerosol into the unit. The DBD tool was placed inside a Bio-Safety Cabinet (Nuaire, Class II, Type A2, Model NU-425–400), and a compressor nebulizer (OMROM compressor nebulizer model NE-C29-E) was attached to the input of the system in order to aerosolize the bacterial particles

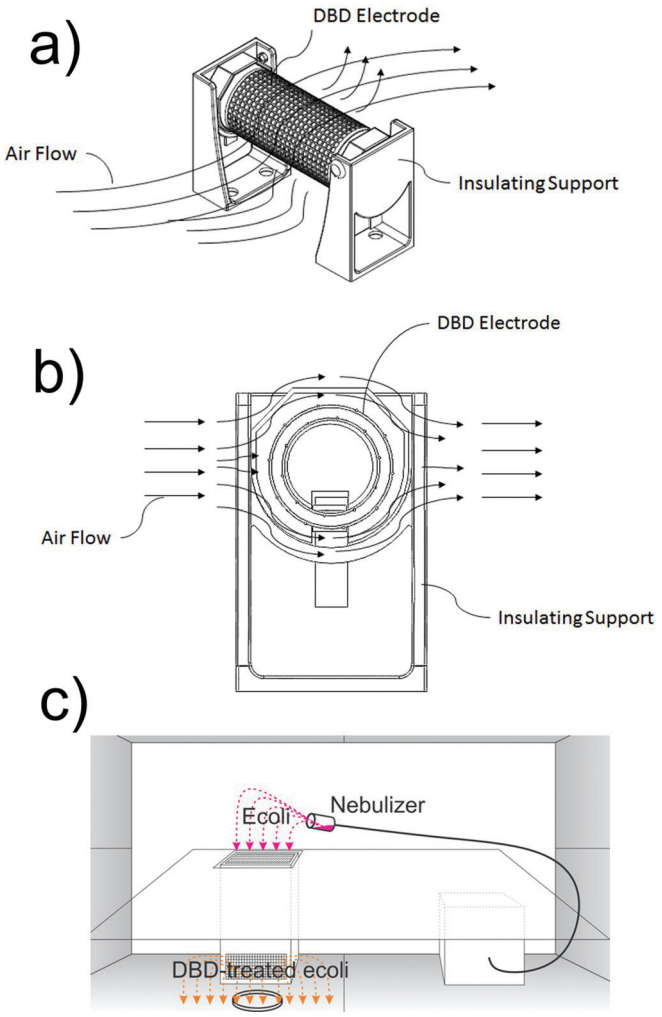

FIG. 1. (a) Schematic of the NV200 DBD system showing the diagram of the assembled coil, (b) cross section illustrating the air flow around the dielectric barrier discharge, and (c) the experimental setup for inactivation *E. coli* and sample collection.

for testing. All vents located on the system were sealed and a platform was placed over the top of the system to ensure the aerosolized particles had a direct route through the system. The bacterial suspension containing *E. coli* and 1 ml of distilled water was transferred to the OMROM compressor nebulizer. The aerosolized particles were fed through the input, and any viable particles were collected at the output in tryptic soy agar plates (BD 236950). The agar plates were left in front of the output of the DBD NV200 tool and were replaced every minute for 5 min. The agar plates were incubated overnight at 37 °C, and after the incubation, colony-forming units (CFU) were observed on the plates, as shown in Fig. 2(a). In these experiments, petri dishes of 100 mm diameter were used with both the fan and electrodes turned ON and OFF simultaneously. The concentration of *E. coli* in each plate was calculated using the following formula: bacteria/ml = number of colonies × dilution of the sample. The log reduction calculation is based on the number of viable microorganisms collected on the plate with and without DBD.

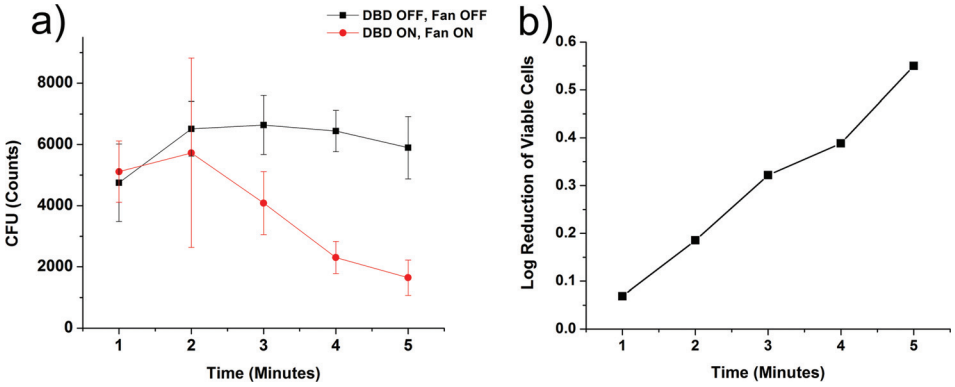

FIG. 2. (a) *E. coli* counts captured from air in an agar plate and recultured. (b) Log reduction of aerosolized *E. coli* upon treatment with DBD.

C. Characterization

For scanning electron microscopy (SEM) imaging, bacterial cells on silicon wafer were fixed in a solution of 2.5% glutaraldehyde (Sigma-Aldrich) in phosphate buffered saline (ATCC) for 2 h and as a second fixative procedure, in a 2% osmium tetroxide (Ted Pella, Inc.) in phosphate-buffered saline for 1.5 h. The samples were then dehydrated in gradually increasing concentrations of ethanol from 60% to 100% in deionized water and chemically dried using hexamethyldisilazane (Sigma-Aldrich) for 5 min. They were placed in a vacuum desiccator overnight in order to prevent reactions with water from humidity. SEM imaging was performed using S4800 scanning electron microscope (Hitachi, Pleasanton, CA). FTIR measurements were carried out using a Perkin Elmer Spectrum GX system. Single side polished silicon wafers were used as substrates for the transmission mode measurement. An untreated silicon substrate was used as a background for the measurement, and each measurement was an average of 200 scans.

The near edge x ray absorption fine spectroscopy (NEXAFS) measurements were performed on beamline 8–2 (bending magnet endstation, spherical grating monochromator) at the Stanford Synchrotron Radiation Lightsource (SSRL).[23] A gold grid in the beam path upstream of the chamber was used for the normalization of the incoming flux. The samples were mounted on an aluminum stick with carbon tape, and all the measurements were done under UHV conditions ($<1\times10^{-8}$ Torr) in a generic XPS/XAS chamber, equipped with a double pass cylindrical mirror analyzer (PHI 15–255 G) mounted perpendicular to the incoming beam axis in the horizontal plane. All measurements were performed at the magic angle (~55° incidence), and the spectrometer detected electrons emitted along the e-vector of the incoming radiation (90° with respect to the incoming light in the horizontal plane). XAS data analysis was performed using Igor Pro. The bacterial samples collected on silicon wafer were freeze-dried using Labconco's FreeZone 4.5 Liter Freeze Dry Systems.

III. RESULTS

Figure 1 shows the schematic of the NV200 DBD system, diagram of the assembled coil, cross section illustrating the airflow around the dielectric barrier discharge, the coil parts, and the experimental setup for airborne inactivation of *E. coli* and sample collection. The bioaerosol containing the nebulized *E. coli* was directed at the top of the DBD tool, which has an internal fan that pulls the contaminated air toward the DBD. The decontaminated air passes out of the bottom outlet. The deactivated bacteria were collected near the outlet in a silicon wafer and agar plates for characterization and reculturing, respectively. The purpose of a partial shield between the nebulizer and the bottom outlet in the DBD tool is to prevent direct settlement of bacteria on the silicon wafer and the culture plate. The DBD design shown in Fig. 1(a) contains metal electrodes separated by a dielectric.

Figure 2 shows the reduction counts of nebulized *E. coli* exposed to DBD; this was collected, recultured, and counted. Comparison of *the E. coli* counts with samples collected in DBD OFF state shows a reduction of air borne *E. coli* exposed to DBD. Figure 2 shows two plots: (a) CFU counts with both fan and electrode were either ON and OFF together and (b) log reduction of viable cells. A similar behavior was observed when the fan was ON throughout the experiment and the electrode was turned ON and OFF independently. In both cases, the DBD ON status results in deactivation of the airborne *E. coli*.

Figure 3 shows the SEM images of the *E. coli* before DBD treatment [Figs. 3(a) and 3(b)] and after DBD treatment [Figs. 3(c)–3(h)]. The nebulized *E. coli* was exposed to DBD and collected from air on a silicon wafer. Upon fixing of the microbes using the procedure described in Sec. II earlier, SEM imaging of several sets of samples was done to study the effect of DBD on the airborne bacteria. The DBD alters the topographical features of *E. coli* to a significant extent ranging from formation of big holes to severe structural deformation resulting in cell death. Physical distortion to the bacterial cell wall happens to varying degrees. It is hypothesized that the degree of distortion depends on the proximity of the bacteria to the electric field and the plasma discharge source. Structural deformation of sterilized *E. coli* similar to our observation has been reported by others using techniques such as biocide emusions[24] and photocatalysis.[25]

The FTIR data for the untreated and DBD-treated *E. coli* are shown in Fig. 4. The peak attributions are made based on

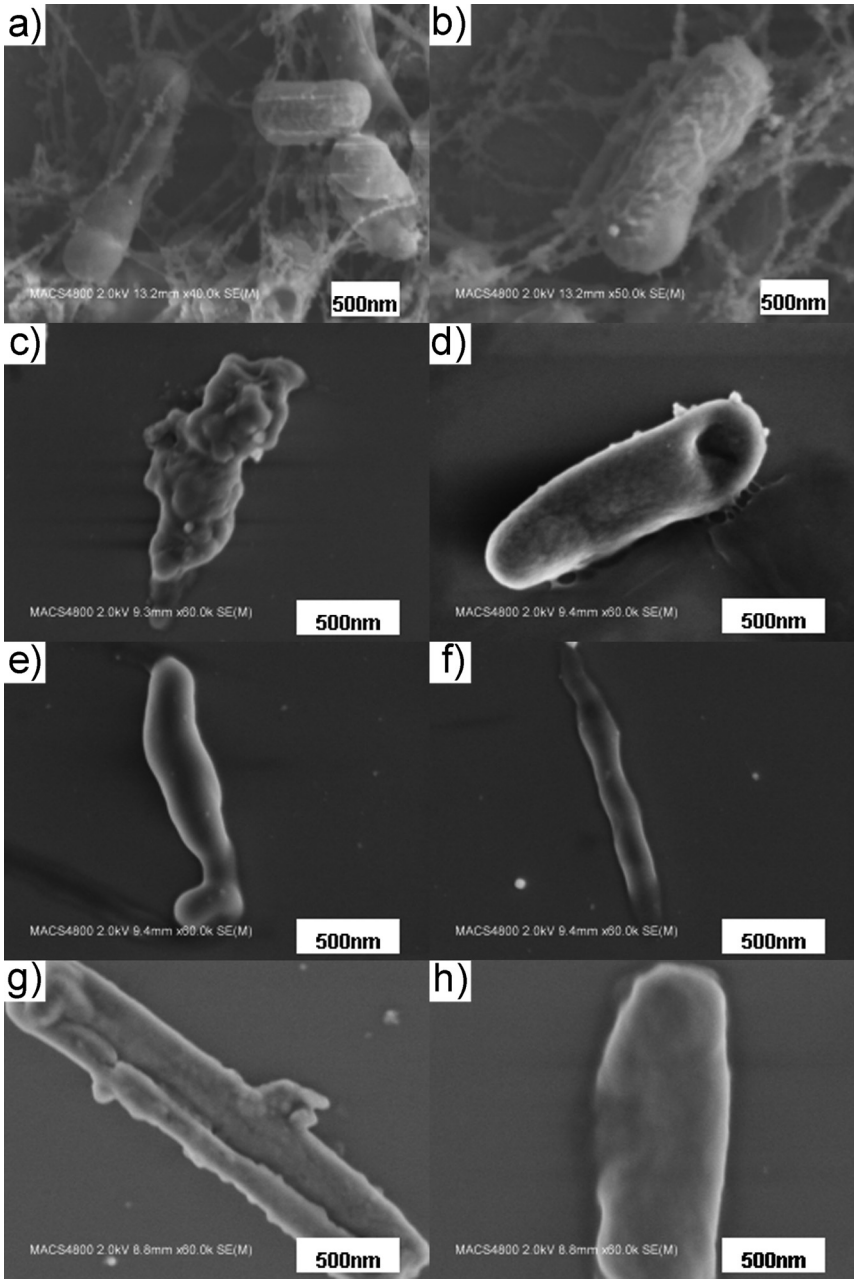

FIG. 3. SEM image of [(a) and (b)] untreated *E. coli* and [(c)–(h)] *E. coli* passed through the DBD and captured from air.

the vast FTIR spectroscopy literature on intact and damaged bacterial cells.[26–31] The broad asymmetric absorption peak between 3000 and 3500 cm^{-1} comprises of multiple bands. Though the peaks were not distinctly resolved, the asymmetric peak shape indicates multiple components including amides and hydrogen bonded OH groups. The characteristic peaks at 3305 and 3066 cm^{-1} are assigned to amide I and amide II, respectively, and the hydrogen bonded OH groups are probably overlapped. The sharp peak centered around 3670 cm^{-1} in the DBD-treated *E. coli* corresponds to the O–H stretching vibration of free OH groups.[32] The sharp peak centered around 2360 cm^{-1} in the DBD-treated *E. coli* is highly likely to be related to isocyanate or carbon double bonded to nitrogen(C=N) bonding.[32] The 1850 cm^{-1} vibration corresponds to symmetric C=0 stretching vibration of the anhydride, and the asymmetric stretching vibration is around 1804 cm^{-1} appearing as a shoulder.[33,34] The absence of this peak in the untreated *E. coli* and the strong vibration observed upon DBD treatment is an indication that this chemical functionality is a product of interaction of the *E. coli* with reactive species generated by the DBD.

A shoulder peak observed around 1730 cm^{-1} corresponds to C=O stretching vibrations of ester functional groups. The vibration bands centered around 1653 and 1550 cm^{-1} correspond to amide vibrations. The amide I band centered around 1653 cm^{-1} is attributed to C=O stretching vibration of amides.[35–37] The amide II band centered around 1550 cm^{-1} band is attributed to N–H deformation of amides

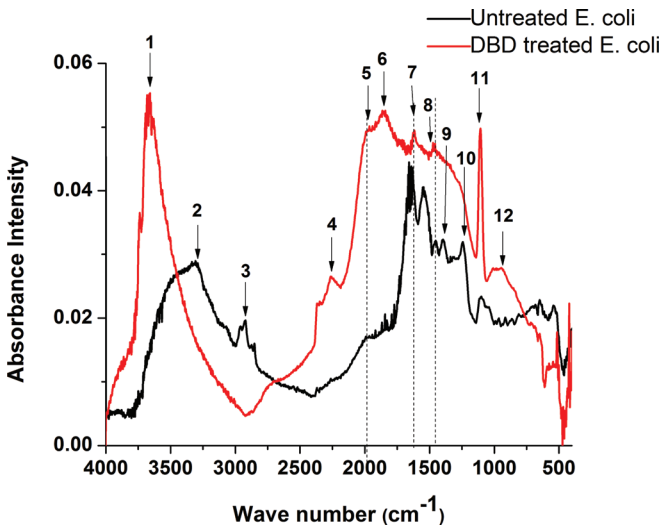

FIG. 4. FTIR spectroscopy analysis of untreated and DBD-treated *E. coli* with peak attribution. 1: Free OH functionalities formed due to oxidation of hydrocarbons; 2: vibrations of amine functionalities (amine and amide) overlapped with hydrogen bonded OH functionality; 3: alkyl CH_2 and CH_3 vibrations; 4: isocyanate or C=N functionality; 5: unknown; 6: acid anhydride formed due to DBD treatment; 7: vibrations of amine functionalities (amine and amide); 8 and 9: CH vibration; 10: phosphate groups present in cell membrane; 11: P=O, C–O–C, and C–O–P; and 12: OH functionality.

including contributions from the C–N stretching vibrations. The absorption peaks between 2800 and 3000 cm^{-1} correspond to the stretching vibrations of alkyl groups (CH_2 and CH_3). The peaks at 2960 and 2923 cm^{-1} correspond to asymmetric stretching vibration of CH_3 and CH_2 and 2870 and 2851 cm^{-1} correspond to symmetric stretching vibration of CH_3 and CH_2, respectively. The peaks at 1460 and 1394 cm^{-1} correspond to CH_3 and CH_2 asymmetric and symmetric. The presence of a band at 1402 cm^{-1} has been attributed to the C–O stretching vibration of carboxylic groups.[38] The peak at 1240 cm^{-1} is due to the P=O asymmetric stretching mode.[39] The region between 1000 and 1100 cm^{-1} with peaks centered around 1040 and 1100 cm^{-1} has multiple components corresponding to the C–O–C and C–O–P stretching and P=0 symmetric stretching vibrations. The peak at 1033 cm^{-1} is attributed to C–OH. The carbonyl C=O stretching vibrations of esters and carboxylic groups, in general, appear around 1740 cm^{-1}. Appearance of a new band around 930 cm^{-1} in the DBD treated *E. coli* is due to the formation of OH species caused by oxidation. An adjacent peak around 956 cm^{-1} is attributed to asymmetric stretching vibration of O–P–O functionalities.

The core level K-edge NEXAFS spectra of carbon, nitrogen, and oxygen are displayed in Fig. 5 for the untreated *E. coli* as well as for two DBD-treated *E. coli* samples with different degrees of damage. The sensitivity of NEXAFS to the local chemical environment and the building block character of the spectroscopy allow us to evaluate the main functional groups and their chemical sensitivity to the DBD treatment. It is important to note that due to the presence of carbon and oxygen contaminants both from the ambient exposure and natively at the silicon substrate surface, the absolute spectral contribution of the *E. coli* relative to the substrate and absorbed contaminants is not very well defined for carbon and oxygen, whereas the differences between the untreated and DBD-treated samples is a robust experimental observation.

In the carbon spectra [Fig. 5(1)], we observe a low energy peak at 285.2 eV in all the samples that corresponds to π^* C=C transitions.[40] We also observe a lower energy shoulder at 284.6 eV that might result from normalization artifacts since it coincides with the carbon "dip" from the beamline optics. A shoulder around 287.4 eV in all the samples reflects C–H resonances of aliphatic carbon. The sharp and high intensity peak at 288.4 eV in untreated *E. coli* can be assigned to π^*C=O transitions associated with either carboxylic groups (COOH) or the carbonyl core in $CONH_2$.[41] The shift by 0.2 eV in DBD-treated *E. coli* indicates an increased electronegativity in the chemical environment of the carbonyl core. This peak attribution is based on the trends in carbonyl core (C=O) π^* transitions, as a function of the electronegativity of the chemical environment, as reported by Urquhart and Ade.[41] Gordon *et al.*, in their study on inner shell excitation spectroscopy of the peptide bonds and proteins, report that the carbonyl core π^* (C=O) transition occurs between 288.2 and 288.6 eV.[42] A low intensity peak seen clearly at 289.4 eV in untreated *E. coli* could be attributed to multiple functional groups that have transitions in this region, e.g., C–H and O-alkyl C groups in polysaccharides or carboxylic acids, or CNH σ^*.[42,43] The broad peaks observed around 291 and 295 eV in all the samples are associated with multiple σ^* components, including C–N in amino acids (~291 eV)[44] and C–O in alcohols and carboxylic acits (~292.5 eV),[45,46] A low intensity peak observed around 297 eV in DBD-treated *E. coli* probably corresponds to σ^*C–OH. A broad excitation centered around 304 eV corresponds to C=C σ^* bonds. The relative intensities of the π^* carbonyl core transition at 288.4 eV and C–O σ^* transition at 292.5 eV show a very clear difference between untreated and DBD-treated *E. coli*. The signal intensity corresponding to C–O σ^* (292.5 eV) is relatively higher in DBD-treated *E. coli* resulting in decreased π^*C=O/σ^*C–O ratio.

The O1s NEXAFS spectra [Fig. 5(2)] display a low energy peak near 531.6 eV for all samples that is associated with the π^* of oxygen double bond functionalities. Based on the energies of 1s->pi* in carbonyl core groups,[41] we can associate this intensity with carboxyl and CONH functionalities (see, for example, Gordon *et al.*, on the O XAS of fibrinogen).[42] A broad peak observed between 536 and 541 eV in untreated *E. coli* could be attributed to multiple components including Rydberg transitions, σ^*O–H and σ^*C–O transitions.[40,42,45] In the DBD-treated *E. coli* these peaks are rather prominent around 537.3 and 539.5 eV, which allow us to assign them primarily to σ^*O–H and σ^*C–O transitions based on the work of Ishii and Hitchcock on carboxylic acids.[47]

In the N K edge spectra [Fig. 5(3)], low intensity peaks in the region of 388.6–389.8 eV correspond to N1s to π^*(N=C) transitions.[48] A high intensity peak at 401 eV corresponds to amide π^* CONH transition. The peak at 405 eV in untreated

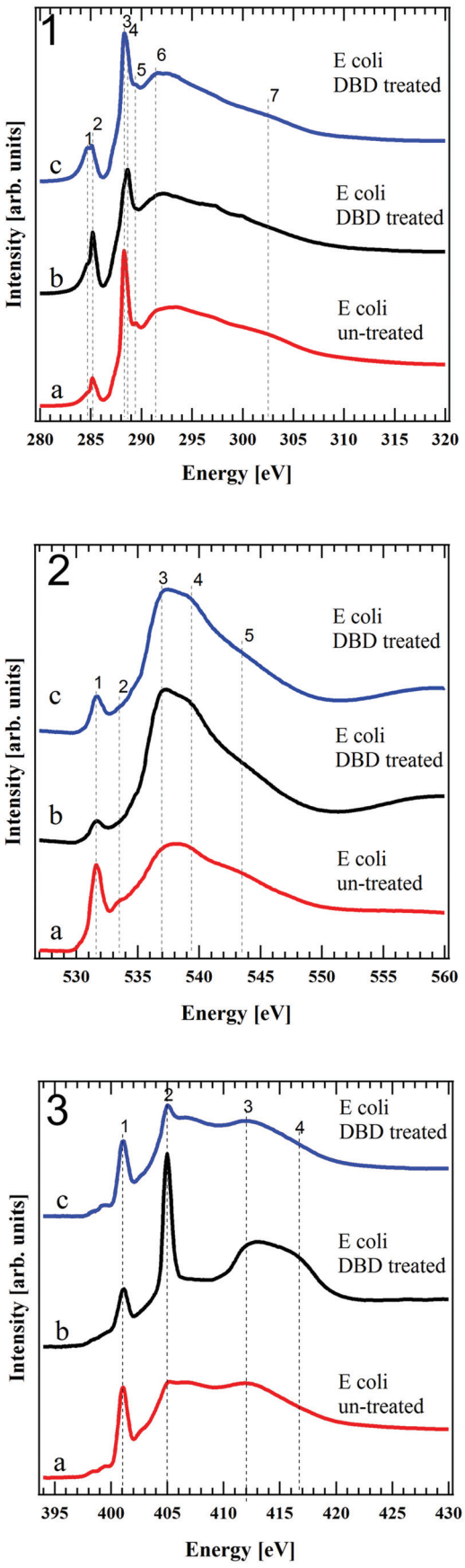

FIG. 5. (1) Carbon (2) oxygen and (3) nitrogen K-edge NEXAFS spectra of (a) untreated and [(b) and (c)] DBD-treated *E. coli*.

E. coli could be due to multiple transitions including π^* of nitro compounds, σ^* N–C and Rydberg transitions.[42,49] However, for the DBD-treated *E. coli,* it can be concluded from the appearance of the peak that it is highly likely to be a π^* transition of nitro compounds. This is in agreement with the literature on nitro compounds.[49,50] The prominent peak centered around 412 eV corresponds to σ^*N=C as observed by Shard *et al.*,[48] The high energy peak around 416 eV which is not present in untreated *E. coli* is likely to be σ^*N=O transition.

IV. DISCUSSION

DBD-based inactivation of the aerosolized *E. coli* as observed in Fig. 2 can be caused by multiple factors. The Gram-negative bacteria contain a cytoplasmic membrane, a peptidoglycan layer, and an outer membrane. The ability of the cell to withstand high internal osmotic pressure and the maintenance of the cell shape is due to the peptidoglycan layer that consists of amino sugars and amino acids.[51,52] The outer membrane contains structural proteins, receptor molecules, and phospholipids and acts as a selective permeability barrier containing hydrophilic diffusion channels.[53–55]

Exposure of the nebulized bacteria in air to DBD resulted in a significant change in chemical structure. The formation of hydrogen bonded and free hydroxyl groups is very evident in DBD treated *E. coli.* An intense peak centered around 3665 cm^{-1} corresponds to free OH functionalities. The hydrogen bonded OH as seen in untreated *E. coli* between 3000 and 3500 cm^{-1} is broad and the sharpness of this peak shifting to higher wave number in the DBD-treated *E. coli* confirms that the OH groups are not hydrogen bonded but are free. Broad feature between 537 and 540 eV, in O XAS, in the untreated *E. coli* can be associated with ether groups (–C–O–C–), and alcohols (-OH) based on comparison with condensed alcohols as well as liquids, for which some degree of hydrogen bonding reduces (-OH) resonance clearly. Pylkkanen *et al.*, in their study on the signature of hydrogen bonding in the oxygen K edge spectrum of alcohols report that hydrogen bonding results in dampening of the pre-edge and broadening of the main edge.[56] Well-defined (-OH) that are separated (as could be expected from repulsion) would give rise to a more distinct peak before the main edge. For DBD-treated *E. coli*, the peaks at 537.3 and 539.5 eV in O XAS, corresponding to σ^*O–H and σ^*C–O transitions, respectively, are prominent with increased intensity, indicating the oxidation of the surface and formation of free OH groups in agreement with the FTIR. In the DBD-treated *E. coli,* the appearance of a new band caused by oxidation has been observed at around 930 cm^{-1} due to the OH species and an adjacent peak around 956 cm^{-1} attributed to asymmetric stretching vibration of O–P–O functionalities. All these observations suggest damage to the outer leaflet of *the E. coli* due to the exposure to the DBD.

It should also be noted that the decreased intensity of π^* CONH transition (C XAS at 288.6 eV, O XAS at 531.6 eV, and N XAS at 401 eV) in DBD-treated *E. coli* correlates well

with the FTIR spectrum where the vibrations corresponding to amide (1650 and 1550 cm^{-1}) decreased in intensity upon DBD treatment. The decreased intensity of the amine and amide vibrations could probably be due to the formation of C=N groups, as observed by the new peak at 2360 cm^{-1}, by replacement of the carbonyl oxygen in amide with nitrogen, probably from the primary amine. A similar observation was seen in N XAS where the transition corresponding to σ*N=C shows high intensity and is prominent in samples treated by DBD.

The DBD-generated reactive species oxidize both alkyl and carbonyl groups. FTIR, C1s XAS, and O XAS confirm the formation of strong saturated functionalities resulting in varying local configurations. O XAS shows formation of single bonded oxygen bonds including OH and CO bonds as evident from strong peaks at 537.3 and 539.5 eV. A sharp rise in 405 eV peak, in N XAS, corresponding to π* transition of nitro group is a clear evidence of oxidation of the cell surface resulting in drastic chemical changes. The role of hydroxyl radicals and reactive oxygen species in *E. coli* inactivation has been studied by several research groups.[57,58] The inactivation mechanism of the reactive oxygen species is based on its effect on cell membrane and intracellular substances. The extent of this molecular damage was assessed using infrared spectroscopy and x ray absorption spectroscopy by observing the bonding environments of carbon, oxygen, and nitrogen. Both the SEM images and the spectroscopic results suggest severe structural deformation as well as surface chemical changes which could have caused bacterial inactivation. An increased presence of oxygenated components including nitro compounds, acid anhydrides and hydroxide groups in the DBD-treated *E. coli* is a strong indication of the role of the DBD-generated reactive oxygen species in causing the chemical changes possibly resulting in cell death.

Airborne microbial load in closed environments including office space and hospitals vary significantly across the world. Reports on air quality studies carried out in hospitals vary from 5 to 25 CFU/m^3 in certain countries to more than 2500 CFU/m^3 in some other countries depending on the personnel density, climate conditions, etc.[59–61] The log reduction reported here is greater than log 0.5 within 5 min of operation. This corresponds to the inactivation of more than 68% of the microbes passed through the DBD system. While this percentage is lower than kill rates quoted by various surface cleaning disinfectants (e.g., 99% or higher), it should be noted that the microbial load for the tests reported here exceeded 10 000 000 CFU/m^3 while the log reduction calculation is based on the number of viable microbes settled on the plate under DBD on and DBD off conditions. Also, the ability of this system to inactivate very low concentration of pathogenic bacteria in real air samples needs to be studied. Though the present initial study demonstrates that the DBD can inactivate the aerosolized *E. coli*, the type of bacteria we have used and the results presented here alone are not sufficient to claim the ability of this system to provide safe environment to hospitals or work places. We have used nonpathogenic biosafety level 1 *E. coli*, but the actual environment in hospitals contains spores, molds, and other robust Gram-positive bacteria in addition to *E. coli*. Further inactivation studies of other types of pathogenic bacteria need to be done to determine the efficacy of the system and the discussion on other pathogens is beyond the scope of this paper.

V. CONCLUSIONS

The effect of dielectric barrier discharge on the morphology and surface chemistry of *E. coli* was studied using electron microscopy, infrared spectroscopy, and x ray absorption spectroscopy. The electromagnetic field around the DBD coil causes severe distortion of the morphology of *E. coli* to varying degrees from formation of pores to shrinking and elongation of the cell structure possibly resulting in leakage of vital cellular materials. The observations made from the core level K-edge NEXAFS spectra of carbon, nitrogen and oxygen correlate well with each other as well as with the FTIR spectra confirming the oxidation, formation of oxygenated components, and chemical modification of the cell structure.

ACKNOWLEDGMENTS

J. Romero-Mangado is a Science and Technology Corporation employee subcontracted to work at NASA Ames Research Center. Ian T. Saunders was a student intern from Norfolk State University. Use of the Stanford Synchrotron Radiation Lightsource, SLAC National Accelerator Laboratory, is supported by the U.S. Department of Energy, Office of Science, Office of Basic Energy Sciences under Contract No. DE-AC02-76SF00515. The authors thank the support from the beamline staff at SSRL, Jun-Sik Lee, and Glen Kerr. The contents of this publication are solely the responsibility of the authors and do not necessarily represent the official views of NIGMS or NIH.

[1]D. B. Graves, J. Phys. D: Appl. Phys. **45**, 263001 (2012).
[2]M. G. Kong, G. Kroesen, G. Morfill, T. Nosenko, T. Shimizu, J. van Dijk, and J. L. Zimmermann, New J. Phys. **11**, 115012 (2009).
[3]G. Isbary, T. Shimizu, Y. F. Li, W. Stolz, H. M. Thomas, G. E. Morfill, and J. L. Zimmermann, Expert Rev. Med. Devices. **10**, 367 (2013).
[4]J. M. Gallagher, N. Vaze, S. Gangoli, V. N. Vasilets, A. F. Gutsol, T. N. Milovanova, S. Anandan, D. M. Murasko, and A. A. Fridman, IEEE Trans. Plasma Sci. **35**, 1501 (2007).
[5]N. D. Vaze, K. P. Arjunan, M. J. Gallagher, V. N. Vasilets, A. Gutsol, A. Fridman, and S. Anandan, "Air and water sterilization using non-thermal plasma," in *IEEE 34th International Conference on Plasma Science, ICOPS 2007* (2007), p. 747.
[6]N. Vaze, S. Park, G. Fridman, and A. Fridman, "Direct exposure to a single filament of DBD plasma leads to the inactivation of airborne bacteria," in *2010 Abstracts IEEE International Conference on Plasma Science* (2010), p. 1.
[7]Y. Liang, *et al.*, Environ. Sci. Technol. **46**, 3360 (2012).
[8]P. E. Hockberger, J. Photochem. Photobiol. **76**, 561 (2002).
[9]A. Davies, T. Pottage, A. Bennett, and J. Walker, J. Hosp. Infect. **77**, 199 (2011).
[10]S. Aiba and A. Yamamoto, Biotechnol. Bioeng. **1**, 129 (1959).
[11]U. S. Roy, J. Gendron, M. C. Delhoménie, L. Bibeau, M. Heitz, and R. Brzezinski, Appl. Microbiol. Biotechnol. **61**, 366 (2003).
[12]Y. Paz, Appl. Catal. B **99**, 448 (2010).

[13]J. Peral, X. Domènech, and D. F. Ollis, J. Chem. Technol. Biotechnol. **70**, 117 (1997).
[14]E. Bermudez, J. B. Mangum, B. A. Wong, B. Asqharian, P. M. Hext, D. B. Warheit, and J. I. Everitt, Toxicol. Sci. **77**, 347 (2004).
[15]S. H. Sharma, Nanomedicine **2**, 753 (2007).
[16]E. Levetin, R. Shaughnessy, C. A. Rogers, and R. Scheir, Appl. Environ. Microbiol. **67**, 3712 (2001).
[17]M. Vleugels, G. Shama, X. T. Deng, E. Greenacre, T. Brocklehurst, and M. G. Kong, IEEE Trans. Plasma Sci. **33**, 824 (2005).
[18]E. Kujundzic, D. A. Zander, M. Hernandez, L. T. Angenent, D. E. Henderson, and S. L. Miller, J. Air Waste Manag. Assoc. **55**, 210 (2005).
[19]A. Pal, S. O. Pehkonen, L. E. Yu, and M. B. Ray, Ind. Eng. Chem. Res. **47**, 7580 (2008).
[20]A. Pal, X. Min, L. E. Yu, S. O. Pehkonen, and M. B. Ray, Int. J. Chem. Reactor Eng. **3**, 1 (2005).
[21]A. Pal, S. O. Pehkonen, L. E. Yu, and M. B. Ray, J. Photochem. Photobiol. A **186**, 335 (2007).
[22]W. J. Kowalski, W. P. Bahnfleth, and T. S. Whittam, Ozone Sci. Eng. **20**, 205 (1998).
[23]K. G. Tirsell and V. P. A. Karpenko, Nucl. Instrum. Methods Phys. Res., Sect. A **291**, 511 (1990).
[24]R. Vyhnalkova, A. Eisenberg, and T. G. M. van de Ven, Langmuir **27**, 11296 (2011).
[25]J. Ren, W. Z. Wang, L. Zhang, J. Chang, and S. Hu, Catal. Commun. **10**, 1940 (2009).
[26]H. M. Al-Qadiri, M. A. Al-Holy, M. Lin, N. I. Alami, A. G. Cavinato, and B. A. Rasco, J. Agric. Food Chem. **54**, 5749 (2006).
[27]J. Schmitt and H. C. Flemming, Int. Biodeterior. Biodegrad. **41**, 1 (1998).
[28]M. Kansiz, P. Heraud, B. Wood, F. Burden, J. Beardall, and D. McNaughton, Phytochemistry **52**, 407 (1999).
[29]L. P. Choo-Smith *et al.*, Appl. Environ. Microbiol. **67**, 1461 (2001).
[30]M. Lin, M. A. Al-Holy, A. Al-Qadiri, D.-H. Kang, A. G. Cavinato, Y. Huang, and B. A. Rasco, J. Agric. Food. Chem. **52**, 5769 (2004).
[31]J. J. Ojeda, M. E. Romero-Gonzalez, R. T. Bachmann, R. G. J. Edyvean, and S. A. Banwart, Langmuir **24**, 4032 (2008).
[32]B. D. Mistry, *A Handbook of Spectroscopic Data Chemistry* (Oxford Book Company, Jaipur, India, 2009).
[33]G. Karakus, A. F. Yenidunya, H. B. Zengin, E. Malatyal, and S. Özçelik, Med. Chem. **1**, 1000103 (2011).
[34]J. Pal, H. Singh, and A. K. Ghosh, J. Appl. Polym. Sci. **92**, 102 (2004).
[35]G. Vedantham, H. G. Sparks, S. U. Sane, S. Tzannis, and T. M. A. Przybycien, Anal. Biochem. **285**, 33 (2000).
[36]J. Kiwi and V. Nadtochenko, Langmuir **21**, 4631 (2005).
[37]A. R. Badireddy, B. R. Korpol, S. Chellam, P. L. Gassman, M. H. Engelhard, A. S. Lea, and K. M. Rosso, Biomacromolecules **9**, 3079 (2008).
[38]V. Guine, L. Spadini, G. Sarret, M. Muris, C. Delolme, J. P. Gaudet, and J. M. F. Martins, Environ. Sci. Technol. **40**, 1806 (2006).
[39]W. Jiang, A. Saxena, B. Song, B. B. Ward, T. J. Beveridge, and S. C. B. Myneni, Langmuir **20**, 11433 (2004).
[40]J. Stewart-Ornstein, A. P. Hitchcock, D. H. Cruz, P. Henklein, J. Overhage, K. Hilpert, J. D. Hale, and R. E. W. Hancock, J. Phys. Chem. B **111**, 7691 (2007).
[41]S. G. Urquhart and H. Ade, J. Phys. Chem. B **106**, 8531 (2002).
[42]M. L. Gordon, G. Cooper, C. Morin, T. Araki, C. C. Turci, K. Kaznatcheev, and A. P. Hitchcock, J. Phys. Chem. A **107**, 6144 (2003).
[43]D. Solomon, J. Lehmann, J. Kinyangi, B. Liang, and T. Schafer, Soil Sci. Soc. Am. J. **69**, 107 (2005).
[44]K. Kaznacheyev, A. Osanna, C. Jacobsen, O. Plashkevych, O. Vahtras, H. Agren, V. Carravetta, and A. P. Hitchcock, J. Phys. Chem. A **106**, 3153 (2002).
[45]D. A. Outka, J. Stohr, R. J. Madix, H. H. Rotermund, B. Hermsmeier, and J. Solomon, Surf. Sci. **185**, 53 (1987).
[46]F. Sette, J. Stohr, and P. A. Hitchcock, J. Chem. Phys. **81**, 4906 (1984).
[47]I. Ishii and A. P. Hitchcock, J. Electron. Spectrosc. Relat. Phenom. **46**, 55 (1988).
[48]A. G. Shard, J. D. Whittle, A. J. Beck, P. N. Brookes, N. A. Bullett, R. A. Talib, A. Mistry, D. Barton, and S. L. McArthur, J. Phys. Chem. B **108**, 12472 (2004).
[49]A. Vairavamurthy and S. Wang, Environ. Sci. Technol. **36**, 3050 (2002).
[50]P. Leinweber, J. Kruse, F. L. Walley, A. Gillespie, K.-U. Eckhardt, R. I. R. Blyth, and T. J. Regier, Synchrotron Radiat. **14**, 500 (2007).
[51]K. H. Schleifer and O. Kandler, Bacteriol. Rev. **36**, 407 (1972).
[52]R. Benz and K. Bauer, Eur. J. Biochem. **176**, 1 (1988).
[53]R. E. Hancock, Trends Microbiol. **5**, 37 (1997).
[54]T. Nakae, J. Ishii, and M. Tokunaga, J. Biol. Chem. **254**, 1457 (1979).
[55]H. Nikaido, Science **264**, 382 (1994).
[56]T. Pylkkanen, J. Lehtola, M. Hakala, A. Sakko, G. Monaco, S. Huotari, and K. Hamalainen, J. Phys. Chem. B **114**, 13076 (2010).
[57]H. Yang, X. Li, Q. Zhao, G. Chen, and C. L. Raston, Environ. Sci. Technol. **46**, 4042 (2012).
[58]P. G. Wu, J. A. Imlay, and J. K. Shang, Biomaterials **31**, 7526 (2010).
[59]K. Qudiesat, K. Abu-Elteen, A. Elkarmi, M. Hamad, and M. Abussaud, Afr. J. Microbiol. Res. **3**, 66 (2009).
[60]M. Augustowska and J. Dutkiewicz, Ann. Agric. Environ. Med. **13**, 99 (2006).
[61]R. Mirzaei, E. Shahriary, M. I. Qureshi, A. Rakhshkhorshid, A. Khammary, and M. Mohammadi, Jundishapur J. Microbiol. **7**, 11688 (2014).